JOURNAL OF SOLID STATE CHEMISTRY 115, 165–173 (1995)

Structural Determination and Magnetic Properties of a New Orthorhombic Chromium Seleno Stannate, $Cr_2Sn_3Se_7$

S. Jobic, F. Bodenan, and G. Ouvrard[1]

Institut des Matériaux de Nantes, Laboratoire de Chimie des Solides, UMR 110 CNRS, 2 rue de la Houssinière, 44072 Nantes Cedex 03, France

and

E. Elkaim and J. P. Lauriat

LURE, Bâtiment 209D, Centre Universitaire Paris-Sud, 91405 Orsay Cedex, France

Received April 21, 1994; in revised form July 11, 1994; accepted July 15, 1994

Since the discovery of a monoclinic phase $Cr_2Sn_3Se_7$, it has been found that, for the same composition, an orthorhombic phase exists. It is described in the *Pnma* space group with $a = 23.097(1)$ Å, $b = 3.8307(2)$ Å, and $c = 12.5414(6)$ Å. The structure, refined to a reliability factor $R_F = 2.4\%$, is built upon $[M_6Se_{14}]^1_\infty$ blocks (M = Cr(III) and Sn(IV)) defining 2,4 tunnels occupied by Sn(II) atoms in bicapped trigonal prisms. The orthorhombic $Cr_2Sn_3Se_7$ structure differs from the monoclinic one through the occurrence of $[M_6Se_{14}]^1_\infty$ blocks instead of $[MSe_2]^2_\infty$ layers. The magnetic susceptibility variation versus the applied magnetic field suggests a spin glass or a superparamagnetism behavior at low temperature. © 1995 Academic Press, Inc.

I. INTRODUCTION

Layered phases are rather attractive compounds in view of their original physical and chemical properties that are not commonly encountered in three-dimensional materials (1–3). That explains why so many studies have been devoted to this particular branch of solid state chemistry. One class of examples is the well-known chalcogenophosphates series M–P–X (4), where the metal phosphorus trichalcogenides gave rise to many studies in relation to either their 2D anisotropic magnetic behavior or the existence of oxidizing centers in the structure allowing these compounds to undergo intercalation reaction involving host/guest redox processes.

The chalcogenophosphates MPX_3 can be viewed as a lamellar transition metal dichalcogenide MX_2 in which one third of M has been replaced by $(P–P)^{VIII}$ pairs (5). Owing to the high oxidation degree of the P_2 pairs, such a substitution lowers correlatively the oxidation state of the transition metal from +IV in the dichalcogenides to +II in the chalcogenophosphates. The lamellar chalcogenide family is so extended to the right of the periodic table, from Ti to Cr for MX_2, to V to Zn for MPX_3. In the phosphorus derivatives, the stabilization of a +III cation can be however achieved through a heterocharge substitution as $M^{I}M'^{III}P_2X_6$ ($CuVP_2S_6$ for example) (6, 7). Such a substitution is not needed if we succeed in replacing P atoms by a IVb main group element. This has been realized in $CrSiTe_3$ (8, 9) and $CrGeTe_3$ (10) which crystallize in a $FePSe_3$ structure type (11). Positive Cr^{3+}–Cr^{3+} magnetic interactions yield a ferromagnetic ordering at 33 and 63 K respectively for the silicon and germanium compounds (12). At the same time, our attempts to prepare new chromium chalcogenides with interesting magnetic properties led to the synthesis and the characterization of $CrSbS_3$ (13) and $CrSbSe_3$ (14), pseudo-monodimensional insulator compounds which undergo, respectively, an antiferromagnetic ordering at about 80 K and a ferromagnetic ordering at 72 K.

As yet, the substitution in the $CrATe_3$ (A = Si, Ge) family of Si and Ge by another IVb element has been unsuccessful, but the series has been extended by considering selenides. Since our attempt to synthesize $CrSnSe_3$ failed, we reported recently the existence of a new mixed valence tin chromium selenide $Cr_2Sn_3Se_7$ (15). Depending on the synthesis conditions, for this stoichiometry two different phases can be obtained which crystallize either in a monoclinic system or in an orthorhombic one, both structures being closely related. This paper will describe the crystal structure and the magnetic properties of the orthorhombic phase.

[1] To whom correspondence should be addressed.

0022-4596/95 $6.00

TABLE 1

Observed and Calculated d Spacings in Å for Orthorhombic-$Cr_2Sn_3Se_7$ (a = 23.097(1) Å, b = 3.8307(2) Å, c = 12.5414(6) Å, and V = 1109.7(2) Å^3) , and Observed and Calculated Intensities Determined from the Lazy Pulverix Program (17)

h	k	l	d_{obs}	d_{calc}	I_{obs}	I_{calc}	h	k	l	d_{obs}	d_{calc}	I_{obs}	I_{calc}
1	0	2	6.05	6.05	12	7	9	1	3	1.8992	1.8993	34	26
2	0	2	5.513	5.511	16	8	10	1	2	1.8861	1.8864	11	11
4	0	2	4.247	4.248	12	6	10	0	4	1.8598	1.8596	6	4
2	0	3	3.930	3.931	22	10	8	1	4	1.8570	1.8575	4	1
6	0	0	3.846	3.850	6	5	1	1	6	1.8290	1.8291	20	16
3	0	3	3.673	3.674	39	19	11	1	1	1.8214	1.8218	4	3
3	1	2	3.0096	3.0090	8	11	10	1	3	1.7880	1.7880	5	5
3	0	4	2.9044	2.9038	66	24	2	0	7	1.7706	1.7705	2	2
8	0	0	2.8868	2.8871	17	8	11	1	2	1.7659	(1.7667	18	5
5	1	1	2.8710	2.8705	46	100	7	0	6		(1.7658		3
4	1	2	2.8456	2.8448	9	11	11	0	4	1.7446	1.7446	8	3
6	0	3	2.8315	2.8318	14	5	6	0	7	1.6243	1.6243	6	2
4	0	4	2.7557	2.7554	100	39	2	1	7	1.6070	1.6071	9	6
6	1	0	2.7155	2.7154	15	27	14	0	2	1.5956	1.5955	17	5
5	1	2	2.6687	2.6684	33	56	6	2	3	1.5866	1.5865	3	1
6	1	1	2.6535	2.6539	7	11	4	2	4	1.5722	1.5727	15	12
8	0	2	2.6233	2.6225	9	4	1	0	8	1.5641	1.5641	5	2
5	0	4	2.5950	2.5942	48	17	13	1	2	1.5612	1.5610	2	3
6	1	2	2.4924	2.4918	14	13	13	0	4	1.5458	1.5458	6	2
7	1	1	2.4522	2.4518	3	3	12	0	5	1.5275	1.5270	8	2
5	1	3	2.4107	2.4096	6	5	6	1	7	1.4953	1.4954	12	7
3	0	5	2.3843	2.3849	9	2	4	2	5	1.4722	1.4720	7	4
2	1	4	2.3745	2.3745	4	4	6	0	8	1.4518	1.4519	6	2
3	1	4	2.3142	2.3141	15	19	16	0	0	1.4434	1.4436	8	4
4	0	5	2.3007	2.3006	29	10	7	0	8	1.4157	(1.4160	15	2
6	1	3	2.2764	2.2772	8	7	10	0	7		(1.4157		2
9	0	3	2.1864	2.1871	14	5	10	2	3	1.3906	1.3904	7	3
10	0	2	2.1670	2.1674	33	13	2	0	9	1.3831	1.3835	6	1
8	0	4	2.1236	2.1239	5	3	9	0	8	1.3379	1.3378	13	4
0	1	5	2.0990	2.0985	15	13	7	1	8	1.3282	1.3282	6	4
0	0	6	2.0910	(2.0902	19	3	15	1	4	1.3004	1.3001	2	4
1	1	5		(2.0899		1	4	1	9	1.2771	1.2771	5	2
1	0	6	2.0818	2.0817	10	3	6	1	9	1.2397	(1.2398	4	2
2	1	5	2.0652	2.0647	16	15	15	0	6		(1.2397		2
8	1	3	2.0201	2.0190	26	4	5	3	1	1.2251	1.2249	10	5
7	0	5	1.9973	1.9968	5	3	18	1	0	1.2165	(1.2167	8	1
11	0	2	1.9910	1.9911	13	5	7	2	7		(1.2163		1
4	1	5	1.9716	1.9723	4	4	2	3	3	1.2144	1.2145	6	1
12	0	0	1.9258	1.9248	9	1	6	3	0	1.2118	1.2120	3	2
0	2	0	1.9148	1.9154	12	38	5	0	10	1.2103	1.2103	6	1
5	1	5	1.9097	1.9106	4	4	5	3	2	1.2078	1.2077	4	3

Note. Average 2θ angle deviation: 9/1000°.

II. EXPERIMENTAL

Synthesis and Chemical Analysis

$Cr_2Sn_3Se_7$ was prepared by heating the elements chromium (Koch Light, 99.999%), tin (Koch Light >99%), and selenium (Aldrich >99.999%) in a 2 : 4 : 9 ratio in a sealed evacuated quartz tube at 800°C for 7 days, followed by a 9-day slow cooling to room temperature. Inside the bulk of the resulting crystalline powder, black shiny needle-like air stable crystals had grown. Single crystal semiquantitative microprobe analyses with energy dispersive analysis by X-rays (EDAX) equipped JEOL-JSM35C scanning electron microscope system yielded the chemical formula $Cr_2Sn_3Se_7$ (Cr: 15%, Sn: 26%, Se: 59%), quite compatible with the values obtained from the preliminary $Cr_2Sn_3Se_7$ monoclinic phase studies (Cr: 14%, Sn: 25%, Se: 61%) (15). To date efforts to prepare a pure powder sample from stoichiometric proportions have led to the formation of the monoclinic phase.

Single Crystal Studies and X-Ray Powder Data

From preliminary rotation and Weissenberg films, orthorhombic symmetry was determined with cell parameters $a = 23.29$ Å, $b = 3.85$ Å (needle axis), and $c = 12.77$ Å. The observation of the $(h0l)$ and $(h1l)$ reciprocal planes reveal the existence rules $(hk0)$ $h = 2n$, and $(0kl)$ $k+l = 2n$. These are consistent with the space groups *Pnma* and $Pn2_1a$. Crystals longer than 0.2 mm were systematically twinned. For data recording we concluded with the choice of a small $0.007 \times 0.150 \times 0.007$ mm^3 suitable crystal.

Accurate parameters were determined by least-squares refinement from data collected on a CPS 120 INEL X-ray powder diffractometer using a monochromatized radiation CuK–L_{III} ($\lambda = 1.540598$ Å) and equipped with a position-sensitive detector calibrated with $Na_2Ca_3Al_{12}F_{14}$ as standard (cubic compound with $a = 10.2501(1)$ Å) (16). The refinement of the diagram in the 10–80° 2θ range yields $a = 23.097(1)$ Å, $b = 3.8307(2)$ Å, and $c = 12.5414(6)$ Å with a 2θ average deviation of 9/1000. Table 1 shows the observed and calculated d spacings along with the observed and calculated intensities (17). Large deviations I_{obs} vs I_{calc} are probably due to the sample preferred orientation relative to the one-dimensional character of the crystallites. In addition, we can notice in the bulk the occurrence of an unknown impurity which may correspond to a tin diselenide slightly intercalated by chromium. In view of the starting 2Cr : 4Sn : 9Se element proportions, the occurrence of such a parasitic phase (as previously observed in the $Cr_2Sn_3Se_7$-monoclinic bulk in smaller proportions) is not surprising.

III. X-RAY STRUCTURE DETERMINATION

Successive attempts to record the crystal data on an Enraf-Nonius CAD4 single crystal X-ray diffractometer (λMoK-$L_{II-III} = 0.71069$ Å, with a 2.0 kW tube) were unsuccessful: only high intensity reflections could be measured well and the data were too limited for solving the structure (5110 measured reflections with $1.5° < \theta < 35.0°$ on a hemisphere, but only 161 independent reflections (in the *Pmmm* Laue group) with $I > 3\sigma(I)$). Therefore, the crystal has been transferred to the W22 wiggler beamline on the DCI ring of LURE (1.85 GeV positons, 250 mA average intensity). There, the smaller divergence of the synchrotron X-ray beam (~0.1 mrad) and its higher brilliance allowed us to record a more complete data set with a better peak/background ratio (on a silicon test crystal, a minimum peak width of 0.006° and an improvement factor of 80 of the peak/background ratio have been observed). In the range $0 \le h \le 26$, $-4 \le k \le 3$, and $0 \le l \le 14$, 1198 reflections were collected at the ZrK-absorption edge ($\lambda = 0.6888$ Å) selected by a double Si(111) monochromator. During the experiment, the incident beam was monitored by means of an ionization chamber, and two standard reflections were measured every 10 reflections to correct for intensity fluctuations during the experiment. Generally, an average of 20 reflections per hour were collected and their profiles were always recorded. Since the mean halfwidth value of the diffraction peaks did not exceed 0.06°, we noticed the occurrence of a slight splitting related to a small twinning that we did not take into account. After integration of the peak profiles, scaling of the data was performed following the behavior of two standard reflections (18). An instability factor $P = 1.3\%$ was derived from the fluctuations of the standard intensities leading to a better estimate of the standard deviations of the observations (19). After applying the Lorentz–polarization correction, a set of 1099 Bragg peaks with $I > 3\sigma(I)$ was kept for data analysis. Experimental parameters for the data collection and refinement are presented in Table 2. No absorption correction was applied in view of the crystal size. The structure was determined via direct methods using the SHELXTL structure determination package (20), then refined in the *Pnma* space group using the XTAL3.2 structure determination package (21). Conventional atomic scattering factors were taken from the usual sources. Anomalous parameters are gathered in Table 2. After averaging (792 independent reflections), the structure was refined with chromium in octahedral sites and tin atoms in both octahedral and trigonal prismatic sites. Considering the magnitude of the atomic displacement parameters (ADP) (22), we allowed a statistical "chromium+tin" atom distribution over the octahedral sites with the imposed constraint that the Cr and Sn occupancies at a given site add up to 1 as in the $Cr_2Sn_3Se_7$ monoclinic phase (15). At the same time, we released the occupancy of the Sn trigonal site to lower the ADP. The refinement resulted in reasonable isotropic thermal factors with an R_F-factor equal to 4.2% (42 variables). The refinement of the anisotropic ADPs and an isotropic secondary extinction coefficient (79 variables) led to $R_F = 2.4\%$ and $R_{wF} = 2.9\%$ with EXT = 0.009(2) (21). The final difference electron density map showed meaningless residues in the $-1.35/1.44$ e$^-$/Å^3 range. We ended at the chemical formulation $Cr_{1.87(2)}(Oh)Sn_{1.13(2)}(Oh)Sn_{1.955(6)}(TP)Se_7$ (Oh and TP symbols refer to the occupation of octahedral and trigonal prismatic sites respectively). In the following, we refer to it as $Cr_2Sn_3Se_7$. Tables 3 and 4 list the final position parameters and temperature factors with their estimated standard deviations.

IV. STRUCTURE DESCRIPTION AND DISCUSSION

Figures 1 and 2 show the projection of the structure in the (a,c) plane. For the cation environment, two types of polyhedra are observed: octahedra, occupied statistically by tin and chromium atoms with a chromium occupancy

TABLE 2
Analytical and Crystallographic Data Parameters of the X-Ray Data Collection and Refinement

1. Physical, crystallographic and analytical data
   Formula: $Cr_{1.87(2)}Sn_{3.08(2)}Se_7$
   Molecular weight: 1015.52 g/mole
   Color: black
   Crystal symmetry: orthorhombic Space group: *Pnma*(62)
   Cell parameters at room temperature refined from X-ray powder diagram:
   a = 23.097(1) Å, b = 3.8307(2) Å, c = 12.5414(6) Å
   Volume: V = 1109.7(2) Å^3
   Z = 4
   Density: ρ = 6.08 g/cm^3
   Absorption coefficient: μ = 319.5 cm^{-1}
   Crystal size: <0.007 × 0.150 × 0.007 mm^3

2. Data collection
   Temperature: 293 K
   Radiation: Zr threshold (λ = 0.6888 Å) Monochromator: double Si (1 1 1)
   Scan mode: ω Scan angle: $\Delta\omega$ = 0.42° (70 steps of 0.006°)
   Recording angle range: 1.5°–23.0°
   Standard reflections: (−9 −1 3), (−10 0 −2)
   Periodicity of intensity control: every 10 reflections

3. Refinement conditions
   Investigated reciprocal space: $0 \le h \le 26$, $-4 \le k \le 3$, $0 \le l \le 14$
   Recorded reflections: 1198
   Independent reflections with $I > 3\sigma(I)$: 792
   Refined parameters: 79
   Weighting scheme: $1/\sigma(I)$
   Anomalous parameters:
   Cr: $f' = 0.26$, $f'' = 0.59$
   Sn: $f' = -0.95$, $f'' = 1.355$
   Se: $f' = -0.135$, $f'' = 2.125$

4. Refinement results
   R_p = 2.4% R_{wF} = 2.9% S = 1.81
   Extinction coefficient: EXT(G/10000) = 0.009(2)
   Difference Fourier intensity: +1.44 e^-/Å^3, −1.35 e^-/Å^3

rate ranging from 0.556(5) to 0.720(5) depending on the crystallographic site, and trigonal prisms reserved only for tin atoms. Such a situation has already been described for the $Cr_2Sn_3Se_7$ monoclinic phase.

The orthorhombic $Cr_2Sn_3Se_7$ structure has a skeleton of $[M_6Se_{14}]^1_\infty$ blocks constituted from edge-sharing (MSe_6) octahedra (M = Cr, Sn) (Fig. 2). Such infinite entities are developed along the b-axis. These blocks are linked together through shared corners every two octahedra, hence defining 2,4 tunnels filled by four tin atoms in bicapped trigonal prisms (the m, n notation for a rectangular tunnel refers to the number of octahedra on each side of it). The prismatic environment of Sn is made of four selenium atoms belonging to two different $[M_6Se_{14}]^1_\infty$ blocks and two selenium forming a common edge with the neighboring ($SnSe_6$) prism. The prism containing Sn(1) is bicapped by Se(3) and Se(4) of $[M_6Se_{14}]^1_\infty$ blocks while that of Sn(2) is capped by Se(3) and by Se(7), common to two adjacent prisms. The B_{eq} values, higher for Sn(2) (3.00(3) Å^2) than for Sn(1) (1.86(2) Å^2), may be related to the nature of the capped anions: Se(3) and Se(4) belonging to the skeleton would insure a higher rigidity for Sn(1). Similarly high isotropic equivalent parameters were observed in the monoclinic phase (3.32(8) Å^2 for Sn(2) and 2.33(6) Å^2 for Sn(1)).

From a structural point of view, the two $Cr_2Sn_3Se_7$ compounds are very similar. The difference comes from the occurrence of the $[M_6Se_{14}]^1_\infty$ blocks in the orthorhombic compound instead of $[MSe_2]^2_\infty$ layers in the monoclinic phase (Fig. 3). The crystal refinements ended at the compositions $Cr_{1.87(2)}Sn_{3.08(2)}Se_7$ and $Cr_{1.90(3)}Sn_{3.04(4)}Se_7$ for the orthorhombic and monoclinic forms, respectively. Within error, no distinction in composition can be made between the orthorhombic and the monoclinic phases.

Table 5 presents the interatomic distances and angles corresponding to the cation environment. The tin atoms of the two bicapped trigonal prisms interact differently

TABLE 3
Atomic Coordinates, Equivalent Isotropic Atomic Displacement Parameters and Occupancies

	x	y	z	B_{eq} (Å^2)	τ_{Sn}	τ_{Cr}
M(1)	0.06733(4)	1/4	0.03602(8)	0.88(3)	0.405(5)	0.595(5)
M(2)	0.19259(5)	3/4	0.14865(9)	0.83(3)	0.280(5)	0.720(5)
M(3)	0.18333(4)	3/4	0.76939(8)	0.88(2)	0.444(5)	0.556(5)
Sn(1)	0.15216(3)	1/4	0.47355(7)	1.86(2)	1.005(3)	
Sn(2)	0.99240(5)	1/4	0.33583(8)	3.00(3)	0.950(3)	
Se(1)	0.23747(4)	3/4	0.58957(8)	1.07(2)		
Se(2)	0.13504(4)	3/4	0.96583(8)	1.05(2)		
Se(3)	0.12672(4)	1/4	0.21252(8)	1.10(2)		
Se(4)	0.11532(4)	1/4	0.69427(8)	1.04(2)		
Se(5)	0.00414(5)	3/4	0.12040(7)	1.18(2)		
Se(6)	0.25315(5)	1/4	0.82608(8)	1.26(2)		
Se(7)	0.06238(4)	3/4	0.45597(8)	1.12(2)		

Note. Isotropic equivalent thermal factor defined as $B_{eq} = 4/3 \sum_i \sum_j \beta_{ij} a_i a_j$.

TABLE 4
Anisotropic Atomic Displacement Parameters

	U_{11}	U_{22}	U_{33}	U_{12}	U_{13}	U_{23}
M(1)	0.0097(6)	0.0114(7)	0.0126(6)	0	−0.0025(4)	0
M(2)	0.1000(7)	0.0095(7)	0.0121(7)	0	−0.0019(5)	0
M(3)	0.0104(5)	0.0109(6)	0.0123(6)	0	−0.0002(4)	0
Sn(1)	0.0219(5)	0.0166(5)	0.0324(5)	0	0.0002(4)	0
Sn(2)	0.0477(7)	0.0315(7)	0.0346(6)	0	−0.0087(5)	0
Se(1)	0.0135(6)	0.0129(6)	0.0143(5)	0	−0.0033(4)	0
Se(2)	0.0142(5)	0.0141(6)	0.0116(5)	0	0.0006(4)	0
Se(3)	0.0138(5)	0.0169(6)	0.0111(5)	0	0.0007(4)	0
Se(4)	0.0115(5)	0.0149(6)	0.0132(5)	0	0.0003(4)	0
Se(5)	0.0170(6)	0.0167(7)	0.0112(5)	0	0.0011(4)	0
Se(6)	0.0168(6)	0.0195(7)	0.0117(5)	0	−0.0025(4)	0
Se(7)	0.0131(6)	0.0099(6)	0.0195(6)	0	−0.0015(4)	0

Note. The expression of the general temperature factor is $\exp[-2\pi^2(U_{11}h^2a^{*2} + U_{22}k^2b^{*2} + U_{33}l^2c^{*2} + 2U_{12}hka^*b^* + 2U_{13}hla^*c^* + 2U_{13}klb^*c^*)]$.

with the surrounding selenium atoms. A large dispersion of Sn–Se distances can be noticed with values ranging from 2.8315(9) to 3.446(1) Å for Sn(1), and from 2.902(1) to 3.467(2) Å for Sn(2). Nevertheless, the mean Sn–Se distances (Sn(1)–Se: 3.124(1) Å; Sn(2)–Se: 3.148(1) Å) agree well with the sum of ionic radii of Se^{-II} ($r_{Se^{-II}}$ = 1.98 Å) and tin at the +II oxidation state ($r_{Sn^{II}}$ = 1.27 Å) (23). Similar values are observed in monoclinic $Cr_2Sn_3Se_7$ (Sn(1)–Se: 3.138(3) Å; Sn(2)–Se: 3.147(3) Å) (15).

The cation–anion distances between tin atoms and Se(7) atoms, the latter shared by ($Sn(1)Se_6$) and ($Sn(2)Se_6$) prisms, (Sn(1)–Se(7): 2.8315(9) Å; Sn(2)–Se(7): 2.924(1) Å) and the distances between Sn and one of the capping atoms (Sn(1)–Se(4): 2.896(1); Sn(2)–Se(7): 2.902(1) Å) are extremely short (0.3 Å lower than the sum of ionic radii) and deviate from the other Sn–Se contacts. Such distances could be attributed to highly covalent bonding Sn–Se interactions. However, the occurrence of a lone s^2 pair on Sn sites (Sn^{II}: $4d^{10}5s^2$) suggests the existence of stress in the matter induced by s^2 steric repulsions. Moreover such constraints are revealed in the ($Sn(1)Se_6$) polyhedra by the Se(1)–Se(6) distance (3.312(2) Å) that is much shorter than 3.62 Å, the Se–Se distance associated with a non-interacting selenium–selenium contact observed in $TiSe_2$ (1). However the mean Se–Se distances of the bicapped prisms (3.878(1) Å for Sn(1), and 3.904(1) Å for Sn(2)) agree well with the sum of van der Waals radii (23). The distance dispersion goes with a similar angle dispersion. The *cis* Se–Sn–Se angles of ($SnSe_6$)

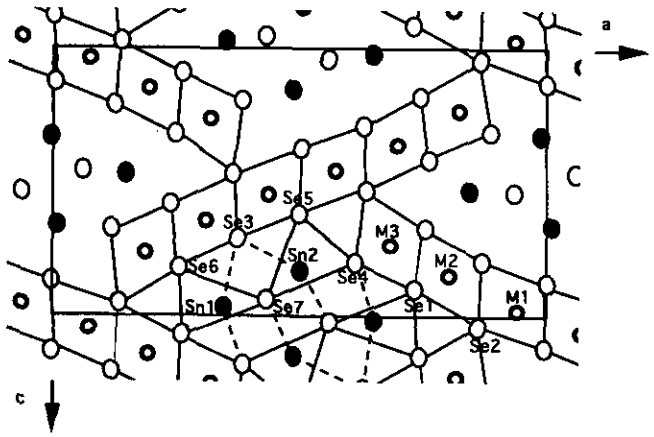

FIG. 1. Projection view in the (*a*, *c*) plane of the orthorhombic arrangement of $Cr_2Sn_3Se_7$ showing the labeling scheme and the unit cell outline.

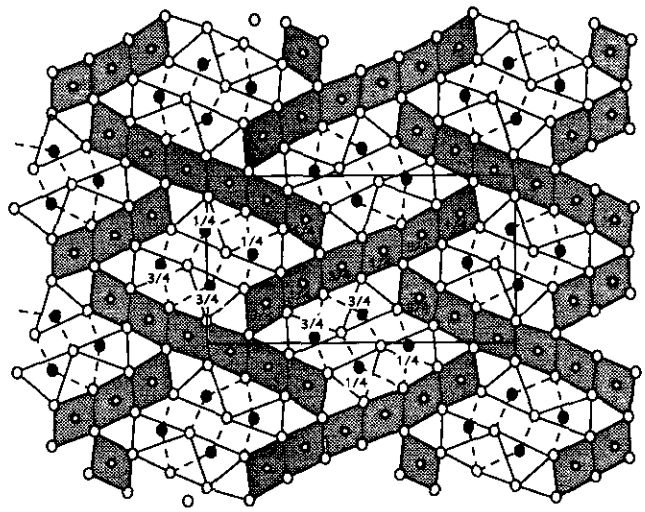

FIG. 2. Enlarged projection view in the (*a*, *c*) plane of the orthorhombic arrangement of $Cr_2Sn_3Se_7$. The shaded area represents the $[M_6Se_{14}]^{II}_{\infty}$ blocks.

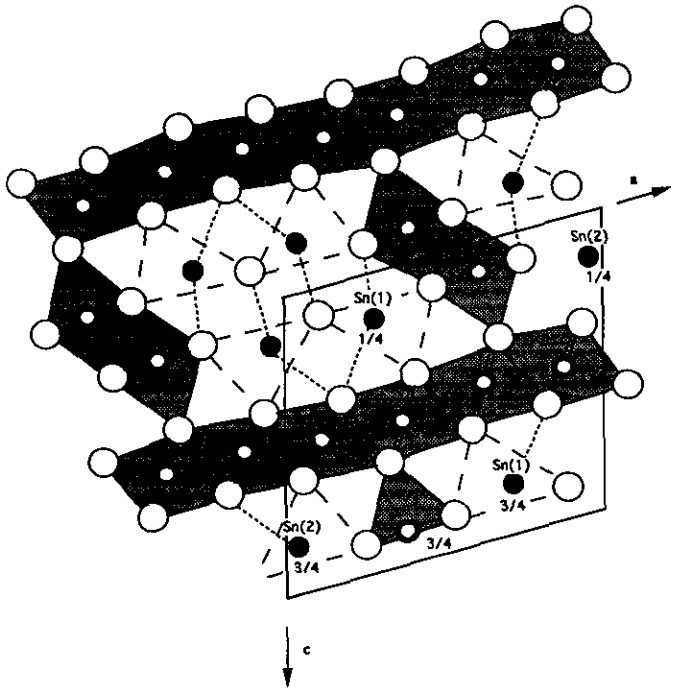

FIG. 3. Projection view in the (a, c) plane of the monoclinic arrangement of $Cr_2Sn_3Se_7$.

prisms range from 60.43(3)° to 94.81(2)° for Sn(1) and from 67.54(3)° to 95.72(1)° for Sn(2).

The occurrence of such distortions with the Sn atoms located far from the center of gravity of the ($SnSe_6$) prisms suggests that the Sn(1) and Sn(2) environment may be considered a hendecahedron rather than a bicapped prism.

Chromium and tin atoms are disordered within octahedra. The mean M–Se distances ($M = x$Cr + $(1 - x)$Sn) are 2.596(1) Å, 2.613(1) Å, and 2.632(1) Å for $M(2)$, $M(1)$ and $M(3)$ respectively, with a rather low dispersion. Analogous values were observed for the $Cr_2Sn_3Se_7$ monoclinic arrangement. Such distances correspond to Cr^{III}–Se ($r_{CrIII} = 0.615$ Å) and to Sn^{IV}–Se ($r_{SnIV} = 0.69$ Å) contacts (23). Note that the mean M–Se distances are not correlated to the Cr-occupancy. Considering the chemical and quantum differences of the elements involved, the statistical distribution of Sn and Cr remains unexplained. However such a phenomenon is not surprising due to the known nature of the preferred environment and size for Cr^{III} and Sn^{IV}. The mean Se–Se distances (3.692(1) Å, 3.670(1) Å, and 3.727(1) Å respectively for $M(1)$, $M(2)$, and $M(3)$ octahedra) reflect no anion–anion interaction though the *cis* Se–M–Se angles deviate from 90° [86.23(2)°–97.30(4)° for $M(1)$, 84.73(2)°–96.17(4)° for $M(2)$, and 86.13(2)°–94.76(4)° for $M(3)$].

From the crystal structure determination and the chemical discussion, the chemical formula can be written

TABLE 5
Mean Interatomic Distances (in Å) and Angles (in °) with Their Estimated Deviations

Bicapped trigonal prismatic sites			
Sn(1)–Se(1) 3.109(1)	×2	Se(1)–Sn(1)–Se(1) 76.05(2)	
Sn(1)–Se(6) 3.446(1)	×2	Se(6)–Sn(1)–Se(6) 67.54(2)	
Sn(1)–Se(7) 2.8315(9)	×2	Se(7)–Sn(1)–Se(7) 85.13(3)	
Sn(1)–Se(3) 3.326(1)		Se(1)–Sn(1)–Se(6) 60.43(3)	×2
Sn(1)–Se(4) 2.896(1)		Se(6)–Sn(1)–Se(7) 92.70(2)	×2
		Se(7)–Sn(1)–Se(1) 94.81(2)	×2
Se(1)–Se(1) 3.8307(2)		Se(3)–Sn(1)–Se(4) 152.73(4)	
Se(6)–Se(6) 3.8307(2)			
Se(7)–Se(7) 3.8307(2)			
Se(1)–Se(6)) 3.312(2)	×2	Mean Sn(1)–Se 3.124(1)	
Se(6)–Se(7) 4.562(1)	×2	Mean Se–Se 3.878(1)	
Se(7)–Se(1) 4.378(1)	×2		
Se(3)–Se(6) 3.660(1)	×2		
Se(3)–Se(7) 3.899(1)	×2		
Se(4)–Se(1) 3.654(1)	×2		
Se(4)–Se(7) 3.754(1)	×2		
Sn(2)–Se(4) 3.162(1)	×2	Se(4)–Sn(2)–Se(4) 74.55(3)	
Sn(2)–Se(5) 3.323(1)	×2	Se(5)–Sn(2)–Se(5) 70.40(2)	
Sn(2)–Se(7) 2.924(1)	×2	Se(7)–Sn(2)–Se(7) 81.84(3)	
Sn(2)–Se(3) 3.467(2)		Se(4)–Sn(2)–Se(7) 95.72(2)	×2
Sn(2)–Se(7) 2.902(1)		Se(7)–Sn(2)–Se(5) 89.79(3)	×2
		Se(5)–Sn(2)–Se(4) 67.54(3)	×2
Se(4)–Se(4) 3.8307(2)		Se(3)–Sn(2)–Se(7) 142.35(4)	
Se(5)–Se(5) 3.8307(2)			
Se(7)–Se(7) 3.8307(2)			
Se(4)–Se(7) 4.516(1)	×2	Mean Sn(2)–Se 3.148(1)	
Se(7)–Se(5) 4.418(1)	×2	Mean Se–Se 3.904(1)	
Se(5)–Se(4) 3.608(1)	×2		
Se(3)–Se(5) 3.608(1)	×2		
Se(3)–Se(7) 3.899(1)	×2		
Se(7)–Se(4) 3.754(1)	×2		
Se(7)–Se(7) 3.632(1)	×2		
Octahedral sites ($M = (1 - x)$Cr + xSn)			
M(1)–Se(2) 2.625(1)	×2	Se(3)–M(1)–Se(2) 88.35(4)	×2
M(1)–Se(3) 2.604(1)		Se(3)–M(1)–Se(5) 87.15(4)	×2
M(1)–Se(5) 2.564(1)		Se(5)–M(1)–Se(2) 97.30(4)	×2
M(1)–Se(5) 2.630(1)	×2	Se(5)–M(1)–Se(5) 87.17(4)	×2
		Se(2)–M(1)–Se(2) 93.73(4)	
Se(3)–Se(2) 3.644(1)	×2	Se(5)–M(1)–Se(5) 93.46(4)	
Se(3)–Se(5) 3.608(1)	×2	Se(2)–M(1)–Se(5) 86.23(2)	×2
Se(5)–Se(2) 3.895(1)	×2		
Se(5)–Se(5) 3.581(1)	×2		
Se(2)–Se(2) 3.8307(2)		Mean M(1)–Se 2.613(1)	
Se(5)–Se(5) 3.8307(2)		Mean Se–Se 3.692(1)	
Se(2)–Se(5) 3.592(1)	×2		
M(2)–Se(1) 2.613(1)	×2	Se(6)–M(2)–Se(1) 86.77(4)	×2
M(2)–Se(2) 2.650(2)		Se(6)–M(3)–Se(3) 91.08(4)	×2
M(2)–Se(3) 2.574(1)	×2	Se(2)–M(2)–Se(1) 93.71(4)	×2
M(2)–Se(6) 2.554(2)		Se(2)–M(2)–Se(3) 88.44(4)	×2
		Se(1)–M(2)–Se(1) 94.29(4)	
Se(6)–Se(1) 3.549(1)	×2	Se(3)–M(2)–Se(3) 96.17(4)	
Se(6)–Se(3) 3.660(1)	×2	Se(1)–M(2)–Se(3) 84.73(2)	×2
Se(2)–Se(1) 3.840(1)	×2		
Se(2)–Se(3) 3.644(1)	×2		
Se(1)–Se(1) 3.8307(2)		Mean M(2)–Se 2.596(1)	
Se(3)–Se(3) 3.8307(2)		Mean Se–Se 3.670(1)	
Se(1)–Se(3) 3.495(1)	×2		

TABLE 5—*Continued*

M(3)–Se(1) 2.579(1)		Se(2)–M(3)–Se(6) 90.38(4)	×2
M(3)–Se(2) 2.704(1)		Se(2)–M(3)–Se(4) 94.55(4)	×2
M(3)–Se(4) 2.650(1)	×2	Se(1)–M(3)–Se(6) 86.47(4)	×2
M(3)–Se(6) 2.603(1)	×2	Se(1)–M(3)–Se(4) 88.66(4)	×2
		Se(4)–M(3)–Se(4) 92.55(4)	
Se(2)–Se(4) 3.933(1)	×2	Se(6)–M(3)–Se(6) 94.76(4)	
Se(2)–Se(6) 3.766(1)	×2	Se(4)–M(3)–Se(6) 86.13(2)	×2
Se(1)–Se(4) 3.654(1)	×2		
Se(1)–Se(6) 3.549(1)	×2		
Se(4)–Se(4) 3.8702(2)		Mean M(3)–Se 2.632(1)	
Se(6)–Se(6) 3.8702(2)		Mean Se–Se 3.727(1)	
Se(4)–Se(6) 3.587(1)	×2		

$[Cr^{III}_{1.87(2)}Sn^{IV}_{1.13(2)}]_{(Oh)}[Sn^{II}_{1.955(6)}]_{(TP)}Se_7$, where the charge balance is realized within error although no constraint was imposed during the crystal structure refinement.

V. MAGNETIC PROPERTIES

Static magnetic susceptibility measurements were performed on a 20.5-mg powder sample using a Quantum Design SQUID magnetometer. Figure 4 shows the reciprocal susceptibility measured between 5 K and room temperature in a magnetic field of 5000 G after a zero field cooling. The susceptibility has been corrected from the diamagnetic contribution using the Pascal constants: $\chi^{dia}_{CrIII} = -15.10^{-6}$ emu, $\chi^{dia}_{SnIV} = -16.10^{-6}$ emu, $\chi^{dia}_{SnII} = -20.10^{-6}$ emu, and $\chi^{dia}_{Se2-} = -48.10^{-6}$ emu. The $1/\chi$ plot shows that the magnetic susceptibility per chromium follows a Curie–Weiss law for temperatures higher than 180 K. Below this temperature, we observe a deviation from Curie–Weiss behavior: the slope decreases and a positive concavity appears in the $1/\chi$ vs T curve. At about 40 K we note the modification of the sign of the concavity. Finally, at low temperatures (about 15 K), we observe a flattened minimum attributable to an antiferromagnetic ordering. The same shape of the $1/\chi = f(T)$ curve was observed for the $Cr_2Sn_3Se_7$ monoclinic arrangement (15). The sample was then composed of 100 needles carefully selected in order to avoid magnetic artifacts. However, magnetic measurements done on the $Cr_2Sn_3Se_7$ monoclinic bulk powder led to the same observations suggesting that the impurity, supposedly a slightly chromium intercalated tin diselenide in both $Cr_2Sn_3Se_7$ samples, is nonmagnetic.

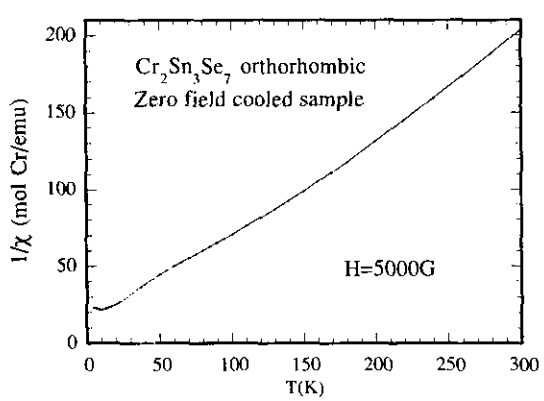

FIG. 4. Reciprocal susceptibility versus temperature for the orthorhombic form of $Cr_2Sn_3Se_7$ (H = 5000 G) after zero field cooling.

From the Curie–Weiss part of the $1/\chi = f(T)$ curve, a Curie constant C = 1.4 emu · K^{-1} · mol^{-1} (μ_{exp} = 3.33 μ_B) can be measured. This value is lower than the spin-only contribution value of 1.9 emu · K^{-1} · mol^{-1} expected for a chromium III cation with a high spin assignment (μ_{the} = 3.87 μ_B) (deduced both from the chemical formula and the X-ray studies). A measured moment of 3.65 μ_B was determined for the $Cr_2Sn_3Se_7$ monoclinic phase (15). For comparison, in $CrSiTe_3$ (9) and $CrGeTe_3$ (10) the corresponding value reaches respectively 3.58 and 3.77 μ_B, while in $CrSbSe_3$ (14) the moment equals 3.90 μ_B. The low Curie constant observed in $Cr_2Sn_3Se_7$ could be due to the simultaneous existence of Cr^{IV} (d^2_{HS}) and Cr^{III} (d^3_{HS}) in the same proportions. Such a hypothesis is in contradiction with the above-mentioned formula. Moreover it is well known that Cr^{IV} is highly unstable in a chalcogen environment and its presence in $Cr_2Sn_3Se_7$ seems doubtful and unrealistic. In a second and more realistic hypothesis, the magnetic moment associated with a high spin d^3 configuration of a chromium cation would undergo a strong reduction due to covalency with surrounding selenium anions. Moreover, as mentioned under Experimental, we noticed the existence of a nonmagnetic impurity in the bulk. Therefore, the magnetic moment deduced from the susceptibility measurements for a $Cr_2Sn_3Se_7$ formula has been underestimated.

The positive paramagnetic temperature which ranges from 12.9 to 19.2 K for the 100–5000 G magnetic field interval, indicates: (i) the occurrence of preponderant ferromagnetic interactions at high temperature, and (ii) the relative weakness of this type of magnetic coupling. Such indirect interactions could be predicted from the observation of the Cr–Cr distances and Cr–Se–Cr angles gathered in Table 6. In fact, for edge-sharing ($Cr^{III}Se_6$) octahedra, the direct $t_{2g} - t_{2g}$ interactions have an antiferromagnetic character while the superexchange interactions via selenium (with a Cr–Se–Cr angle of about 90°) are essentially ferromagnetic. In orthorhombic $Cr_2Sn_3Se_7$, the Cr–Cr distances in $[M_6Se_{14}]^1_\infty$ ranging from 3.746(1) Å (between two adjacent chromium atoms in the (a,c) plane) to 3.8307(2) Å (along the b-axis) seem too large to allow a significant $d_{Cr-t_{2g}}$ overlap. These values are comparable with the parameters observed in $NaCrSe_2$ (d_{Cr-Cr} = 3.73 Å and Cr–Se–Cr angle = 93.5° with J/k = 8 K) which induce ferromagnetic ordering (24).

TABLE 6
Interatomic Cr–Cr Distances (in Å) and Se–Cr–Se Angles (in Degrees) ($M = (1 - x)Cr + xSn$ with $x = 0.405(5)$, $0.280(5)$, and $0.444(5)$ for $M(1)$, $M(2)$, and $M(3)$, Respectively)

Cr–Cr Distances	Cr–Se–Cr Angles
In the (a, c) plane	
$M(1)$–$M(1)$ 3.763(1)	$M(1)$–Se(5)–$M(1)$ 92.83(4)
	$M(1)$–Se(5)–$M(1)$ 92.83(4)
$M(1)$–$M(2)$ 3.746(1)	$M(1)$–Se(2)–$M(2)$ 90.50(4)
	$M(1)$–Se(3)–$M(2)$ 92.68(4)
$M(2)$–$M(3)$ 3.765(1)	$M(2)$–Se(1)–$M(3)$ 92.97(4)
	$M(2)$–Se(6)–$M(3)$ 93.79(4)
Along the b axis	
$M(1)$–$M(1)$ 3.8307(2)	$M(1)$–Se(2)–$M(1)$ 93.73(4)
	$M(1)$–Se(5)–$M(1)$ 93.46(4)
$M(2)$–$M(2)$ 3.8307(2)	$M(2)$–Se(1)–$M(2)$ 94.29(4)
	$M(2)$–Se(3)–$M(2)$ 96.17(4)
$M(3)$–$M(3)$ 3.8307(2)	$M(3)$–Se(4)–$M(3)$ 92.55(4)
	$M(3)$–Se(6)–$M(3)$ 94.76(4)

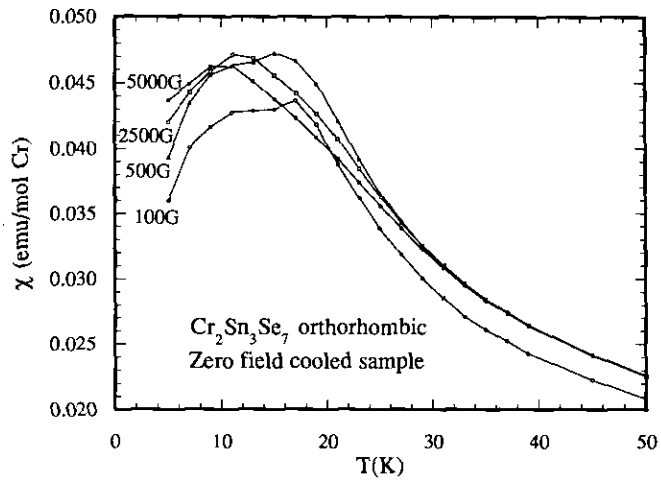

FIG. 5. Temperature dependence of $\chi(T)$ between 0 and 50 K for different applied field strengths (H = 100, 500, 2500, and 5000 G) after zero field cooling.

The simultaneous occurrence of ferromagnetic and antiferromagnetic interactions (at high and low temperatures respectively), expressed with the contradiction between a positive Curie temperature and a minimum in the reciprocal susceptibility, is reminiscent of the $Eu_xSr_{1-x}S$ (25) and $Cu_xCr_xSn_{2-x}S_4$ (26) compounds. Such behavior could suggest a spin glass transition. To envision such an eventuality one needs a refinement of the susceptibility measurements. In fact, spin glass compounds exhibit a maximum in the susceptibility curve at low temperature with characteristics (χ_{max} and T_{max}) that depend strongly on the experimental conditions. To test the model of a spin glass transition in the $Cr_2Sn_3Se_7$ orthorhombic arrangement, we determined the susceptibility for different magnetic fields at low temperature after a zero field cooling (ZFC) and a field cooling (FC). The difficulties in synthesizing the $Cr_2Sn_3Se_7$ orthorhombic compound in sufficient amounts and the existence of a tin diselenide slightly intercalated with chromium as impurity prevent us from using ^{119}Sn Mössbauer spectroscopy to probe any possible spin glass state through the hyperfine field transferred on the tin nuclei.

In Fig. 5 the variation of the ZFC magnetic susceptibility between 0 and 50 K is reported. The lower the applied magnetic field, the more curved the maximum of susceptibility seems. In addition, T_{max} decreases from 15 to 9.5 K when H increases from 100 to 5000 G. This type of

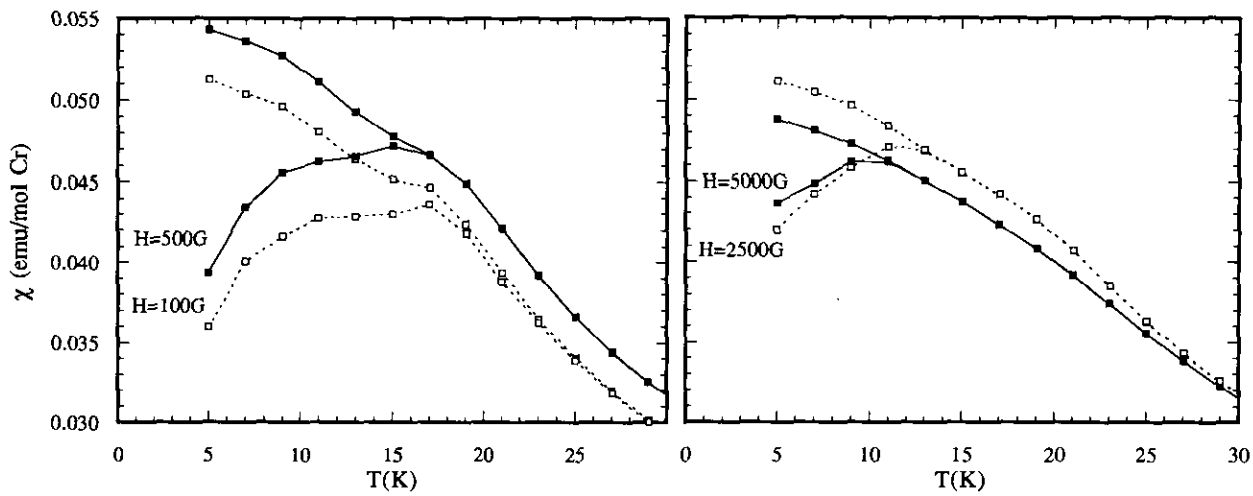

FIG. 6. Susceptibility versus temperature curves after a field cooling and a zero field cooling for H = 100, 500, 2500, and 5000 G.

behavior is characteristic of spin glasses or superparamagnetic compounds. For spin glasses, χ_{max} usually increases with the applied field. Such an evolution is not observed for $Cr_2Sn_3Se_7$: from 100 to 500 G χ increases, then it goes down upon increasing the field further. The variation between 500 and 2500 G remains weak. Such a phenomenon could be related to a saturation process where the grain size becomes smaller than the magnetic domains.

Figure 6 gives the variation of the susceptibility for the ZFC and FC branches. We observe that the irreversible phenomenon showed by the hysteresis of the magnetic susceptibility decreases when the magnetic field increases: the freeze of the magnetic moments can be realized only if the energy associated with the applied field is lower than the energy gap which hinders the spin alignment. At high fields, after a zero field cooling or a field cooling, the susceptibilities have to be equal since the available energy is sufficiently large to avoid a statistical spin orientation. Moreover, the FC branch does not follow the classical evolution of χ for a spin glass with a plateau just below T_g (or T_{max}) (25). In fact we observe a slight increase of χ after the T_g. Such behavior could be attributed to superparamagnetism rather than a spin glass transition. Consequently, the occurrence of isolated chromium clusters cannot be ruled out.

The spin arrangement in and between the $[M_6Se_{14}]^1_\infty$ blocks should be probed by neutron diffraction. In the same way, the occurrence of a spin glass state should be confirmed. However, such a technique requires a large amount of powder. A more thorough investigation of the magnetic state at low temperature will depend upon the development of the synthesis process or the crystal growth.

ACKNOWLEDGMENT

We are grateful to Dr. P. Molinié for his assistance with magnetic susceptibility measurements.

REFERENCES

1. F. Lévy (Ed.), *in* "Physics and Chemistry of Materials with Layered Structures 2." Reidel, Dordrecht, Holland, 1976.
2. P. Monceau (Ed.), *in* Physics and Chemistry of Materials with Low-Dimensional Structures Series B; Parts 1 and 2. Reidel, Dordrecht, Holland, 1985.
3. J. Rouxel (Ed.), *in* "Physics and Chemistry of Materials with Low-Dimensional Structures Series B," Reidel, Dordrecht, Holland, 1986.
4. R. Brec, *Solid State Ionics* **22,** 3 (1986).
5. G. Ouvrard and R. Brec, *Eur. J. Solid State Inorg. Chem.* **27,** 477 (1990).
6. S. Lee, G. Ouvrard, P. Colombet, and R. Brec, *Mater. Res. Bull.* **21,** 917 (1986).
7. G. Burr, E. Durand, M. Evain, and R. Brec, *J. Solid State Chem.* **103,** 514 (1993).
8. G. Ouvrard, E. Sandré, and R. Brec, *J. Solid State Chem.* **73,** 27 (1988).
9. R. E. Marsh, *J. Solid State Chem.* **77,** 190 (1988).
10. V. Carteaux, Thesis, University of Nantes, France, 1992.
11. W. Klingen, G. Eulenberger, and H. Hahn, *Z. Anorg. Allg. Chem.* **401,** 97 (1973).
12. V. Carteaux, G. Ouvrard, J. C. Grenier, and Y. Laligant, *J. Magn. Mag. Mater.* **94,** 127 (1991).
13. S. Jobic, P. Le Boterf, F. Bodénan, and G. Ouvrard, *C.R. Acad. Sci.* **318,** 893 (1994).
14. D. Odink, V. Carteaux, C. Payen, and G. Ouvrard, *Chem. Mater.* **5,** 237 (1993).
15. S. Jobic, P. Le Boterf, R. Brec, and G. Ouvrard, *J. Alloys Comp.* **205,** 139 (1994).
16. P. Deniard, M. Evain, J. M. Barbet, and R. Brec, *Mater. Sci. Forum* **79–82,** 363 (1991).
17. R. Yvon, W. Jeitschko, and E. Parthé, *J. Appl. Crystallogr.* **10,** 73 (1977).
18. R. Blessing, *Crystallogr. Rev.* **1,** 3 (1987).
19. L. E. McCandlish, G. H. Stout, and L. C. Andrews, *Acta Crystallogr. Sect. A* **31,** 245 (1975).
20. "SHELXTL PLUS: Structure Determination Package," Siemens Analytical X-Ray Instruments, Inc., 1990.
21. S. R. Hall, H. D. Flack, and J. M. Stewart (Eds.), "Xtal3.2 Reference Manual," Universities of Western Australia, Geneva, and Maryland, 1992.
22. W. F. Kuhs, *Acta Crystallogr. Sect. A* **48,** 80 (1992).
23. R. D. Shannon, *Acta Crystallogr. Sect. A* **32,** 751 (1976).
24. F. M. R. Engelsman, G. A. Wiegers, F. Jellinek, and B. Van Laar, *J. Solid State Chem.* **6,** 574 (1973).
25. H. Maletta and W. Felsch, *Z. Phys. B* **37,** 55 (1980).
26. P. Colombet, M. Tremblet, and M. Danot, *Phys. Status Solidi* **72,** 105 (1982).